THE JOURNAL OF PHYSICAL CHEMISTRY C

Article

pubs.acs.org/JPCC

Molecular Electronic Coupling Controls Charge Recombination Kinetics in Organic Solar Cells of Low Bandgap Diketopyrrolopyrrole, Carbazole, and Thiophene Polymers

Teresa Ripolles-Sanchis,[†] Sonia R. Raga,[†] Antonio Guerrero,[†] Matthias Welker,[‡] Mathieu Turbiez,[‡] Juan Bisquert,[†] and Germà Garcia-Belmonte*[,†]

[†]Photovoltaic and Optoelectronic Devices Group, Departament de Física, Universitat Jaume I, ES-12071 Castelló, Spain

[‡]BASF Schweiz AG, Schwarzwaldallee 215, CH-4002 Basel, Switzerland

Supporting Information

ABSTRACT: Low-bandgap diketopyrrolopyrrole- and carbazole-based polymer bulk-heterojunction solar cells exhibit much faster charge carrier recombination kinetics than that encountered for less-recombining poly(3-hexylthiophene). Solar cells comprising these polymers exhibit energy losses caused by carrier recombination of approximately 100 mV, expressed as reduction in open-circuit voltage, and consequently photovoltaic conversion efficiency lowers in more than 20%. The analysis presented here unravels the origin of that energy loss by connecting the limiting mechanism governing recombination dynamics to the electronic coupling occurring at the donor polymer and acceptor fullerene interfaces. Previous approaches correlate carrier transport properties and recombination kinetics by means of Langevin-like mechanisms. However, neither carrier mobility nor polymer ionization energy helps understanding the variation of the recombination coefficient among the studied polymers. In the framework of the charge transfer Marcus theory, it is proposed that recombination time scale is linked with charge transfer molecular mechanisms at the polymer/fullerene interfaces. As expected for efficient organic solar cells, small electronic coupling existing between donor polymers and acceptor fullerene (V_{if} < 1 meV) and large reorganization energy ($\lambda \approx 0.7$ eV) are encountered. Differences in the electronic coupling among polymer/fullerene blends suffice to explain the slowest recombination exhibited by poly(3-hexylthiophene)-based solar cells. Our approach reveals how to directly connect photovoltaic parameters as open-circuit voltage to molecular properties of blended materials.

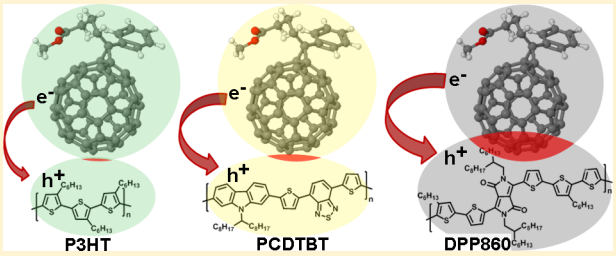

1. INTRODUCTION

Organic photovoltaic technology can potentially reduce production costs of solar energy by adopting cheaper printing technologies. New insights on materials properties and interface engineering have led very recently to achieve power conversion efficiencies near 10% in the case of bulk-heterojunction solar cell structures.[1] Improvement in solar cell efficiency partially relies upon achieving higher open-circuit voltages V_{oc} by limitation of the charge carrier recombination flux,[2] which is understood as the process of charge transfer occurring between occupied acceptor levels and unoccupied donor states. By inhibiting recombination current to some extent the amount of charge carriers involved in the photovoltaic operation is enhanced. This produces an enlarged offset in the separate carrier Fermi levels, E_{Fn} and E_{Fp} for electrons and holes, that finally is measured as an output voltage,[3]

$$qV_F = E_{Fn} - E_{Fp} \quad (1)$$

The Fermi level position is highly dependent on the actual energy distribution of electronic states DOS within the effective bandgap $E_g \approx E_{LUMO}(A) - E_{HOMO}(D)$. The energetically disordered environment spreads the DOS forming large electronic distributions within the bandgap. But even more important is chemical interactions that tend to aggregate molecular units in extended clusters with altered DOS.[4] The occurrence of aggregates is known to be highly influenced by the processing conditions followed during the cell construction.[5] For instance, the use of different solvents is critical in establishing the final DOS of both acceptor and donor molecular constituents.[6] The interplay between materials energetics and charge recombination kinetics does establish the achievable open-circuit voltage. Hence practical knowledge might be gained if a separation between the repercussion on V_{oc} of energetics from recombination kinetics is accomplished in complete devices after materials processing.[7]

The rate limiting mechanism governing the kinetics of charge carrier recombination in organic solar cells is still uncertain. Some models regard recombination as a transport-controlled process in similarity to that occurring in single phase organic compounds,[8] and express it by means of Langevin-like

Received: March 20, 2013
Revised: April 2, 2013
Published: April 2, 2013

   dx.doi.org/10.1021/jp402751v | J. Phys. Chem. C 2013, 117, 8719−8726

recombination coefficients B_L directly related to the carrier mobility μ of electrons and holes as $B_L = q\mu/\varepsilon$ (ε being the effective permittivity of the blend).[9] However, such models establish a strong correlation between transport, mobility properties, and recombination kinetics, which is rarely observed from separate determinations of the recombination coefficient B and μ. Instead, we conclude that the time scale for charge recombination is linked with charge transfer molecular properties at the donor/acceptor interface rather than with transport characteristics before separate carriers meet each other. Recent papers have explicitly suggested, following different approaches, that charge recombination is closely related to molecular interfacial properties.[10] Particularly interesting are theoretical findings observing a high dependence of the charge transfer event kinetics on the relative molecular orientations and intermolecular distances.[11] Recalling the Marcus approach for electronic charge transfer, we have ascertained that differences in charge recombination among different acceptor/donor combinations are related to variations in the electronic coupling matrix, while all investigated blends exhibit a relatively high reorganization energy $\lambda \approx 0.7$ eV. Our findings reveal that blend properties rather than energetic characteristics of individual constituents determine losses caused by charge recombination.

To evaluate the role of the charge carrier recombination kinetics on the achievable open-circuit voltage of polymer/fullerene solar cells and separate it from that owed to the donor HOMO position, we have analyzed the device performance by using a purely electrical technique based on impedance measurements of complete cells under illumination. Performance is compared of solar cells comprising [6,6]-phenyl-C_{71}-butyric acid methyl ester ($PC_{70}BM$) as acceptor fullerene and different donor polymers: namely, poly(3-hexylthiophene (P3HT), poly[[9-(1-octylnonyl)-9H-carbazole-2,7-diyl]-2,5-thiophenediyl-2,1,3-benzothiadiazole-4,7-diyl-2,5-thiophenediyl] (PCDTBT),[12] and low bandgap diketopyrrolopyrrole-oligothiophene copolymer (DPP860, see Figure 1). We have identified polymer HOMO levels that govern the photovoltaic operation of the active blend by determining the rise of the capacitance at forward voltage. Carrier recombination current is evaluated from the analysis of the resistive response. Energy losses expressed as reduction in V_{oc} amount to approximately 100 mV for increments in recombination coefficient of about 1 order of magnitude in the case of DPP860 or PCDTBT in comparison with P3HT. Such reduction is finally originated by a slightly stronger electronic coupling. Impedance measurements allow determining relevant effects influencing V_{oc}, and connects them to microscopic, molecular parameters. Our approach can be used as an orienting guide for further solar cell improvement in combination with morphological and theoretical data.

2. EXPERIMENTAL SECTION

Materials. P3HT (Luminescence Technology Corp.), PCDTBT (1-Material), $PC_{70}BM$ (Nano-C, 99%), PEDOT/PSS (CLEVIOS P AI 4083), *o*-dichlorobenzene (Aldrich, 99.9%), chloroform (Aldrich, 99.9%), Ca (Aldrich, 99.995%), and silver (Aldrich, 99.99%) were used as received without further purification. DPP860 was synthesized following a similar route, as previously reported for PDPP5T[13] with slight variations concerning the alkyl chains attached to the thiophene units, and was supplied by BASF (see Figure 1). All manipulations were carried out in a glovebox under a nitrogen

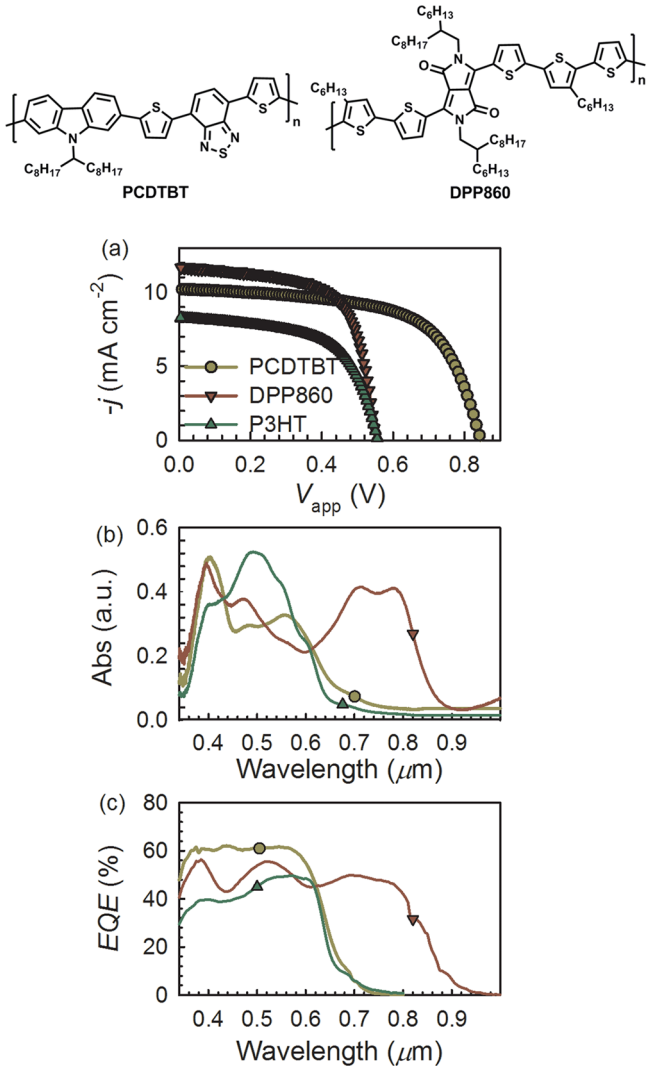

Figure 1. (a) Current density−voltage characteristics of typical devices ITO/PEDOT:PSS/polymer:$PC_{70}BM$/Ca/Ag using P3HT, PCDTBT, and DPP860 as polymer donors. (b) Absorption and (c) external quantum efficiency spectra showing the difference between small (DPP860) and large bandgap (P3HT and PCDTBT) donors.

atmosphere unless otherwise stated. P3HT/$PC_{70}BM$ solutions (1:1 ratio) were prepared in *o*-dichlorobenzene (17 mg/mL) and were stirred at room temperature. PCDTBT/$PC_{70}BM$ solutions (1:4, 4 mg/mL) were prepared in a chlorobenzene/1,2-dichlorobenzene (1:2.5 volume ratio) mixture and were stirred at 70 °C. DPP860/$PC_{70}BM$ (1:2, 7.5 mg/mL) were prepared in a 1,2-dichlorobenzene/chloroform mixture (1:9 volume ratio) and were stirred at 55 °C. All solutions were stirred at the mentioned temperature for at least 16 h prior to device fabrication and were cooled down to room temperature 5 min before use.

Device Fabrication. Polymer solar cells were fabricated with a standard sandwich structure of ITO/PEDOT:PSS/donor:$PC_{70}BM$/Ca/Ag and 9 mm^2 of active area. PEDOT/PSS was spin coated in air at 5500 rpm for 30 s onto an ITO-coated glass substrate (10 Ohm/sq), film thickness of ~35 nm. The substrates were heated at 120 °C for 10 min to remove traces of water and were transferred to a glovebox equipped with a thermal evaporator. The P3HT/$PC_{70}BM$ layer was deposited at speeds of 1200 rpm (thickness was about 110 nm) for 30 s,

dx.doi.org/10.1021/jp402751v | J. Phys. Chem. C 2013, 117, 8719−8726

Table 1. Photovoltaic Parameters and Parameters Extracted from Impedance Spectroscopy Analysis of Polymer/$PC_{70}BM$ Solar Cells[a]

	j_{sc} (mA cm^{-2})	V_{oc} (mV)	FF	PCE (%)	α	β	γ	E_{HOMO} (eV)
P3HT	8.36	560	0.59	2.7	0.35	0.71	2.01	−5.4
PCDTBT	10.21	845	0.62	5.4	0.32	0.68	2.00	−5.8
DPP860	12.80	554	0.66	4.7	0.44	0.78	1.77	−5.5

[a]Polymer E_{HOMO} extracted from capacitance plot in Figure 2b assuming the value for P3HT determined from voltammetry methods (Supporting Information).

followed by a slow drying of the film in a Petri dish. At this point, P3HT/$PC_{70}BM$ devices were thermally annealed at 130 °C for 20 min. Devices based on PCDTBT/$PC_{70}BM$ blends were spin-coated at 1000 rpm for 60 s (~100 nm) and films were thermally annealed at 70 °C for 30 min. Finally, DPP860/$PC_{70}BM$ blends were spin-coated over prerotating substrates at a speed of 7500 rpm; 25 μL of solution was used for 2 × 2 cm substrates to provide a ~50 nm active layer thickness, and no additional drying step was required. Evaporation was carried out for all samples at a base pressure of 3 × 10^{-6} mbar, and Ca (10 nm) and Ag (100 nm) were sequentially evaporated. The top Ca/Ag electrodes were then encapsulated with epoxy and a glass slide before testing.

Device Characterization. Current density−voltage and impedance measurements were carried out by illumination with a 1.5G illumination source (1000 W m^{-2}) using an Abet Sun 2000 Solar Simulator. The light intensity was adjusted with a calibrated Si solar cell. Impedance spectra were recorded by applying a small voltage perturbation (20 mV rms) at frequencies from 1 MHz to 1 Hz. Measurements were carried out under 1 sunlight intensity sweeping the DC voltage in the range 0 to V_{oc}. These measurements were performed with Autolab PGSTAT-30 equipped with a frequency analyzer module. Recombination resistance R_{rec} and chemical capacitance C_μ were directly extracted from the low-frequency region, as previously reported.[14]

3. RESULTS AND DISCUSSION

DOS and Capacitance Response. Solar cells of structure indium tin oxide (ITO)/poly(3,4-ethylenedioxythiophene)/poly(styrene sulfonic acid) (PEDOT/PSS)/polymer/$PC_{70}BM$/Ca/Ag, were prepared as described in the Experimental Section. To test the effect of the donor LUMO level shift on the overall recombination kinetics and open-circuit voltage, three different donor polymers have been analyzed: namely, P3HT, PCDTBT, and DPP860. Impedance spectroscopy measurements were performed with Autolab PGSTAT-30 by applying a small ac perturbation to maintain the linearity of the response, as described in previous work.[7a]

An example of the measured current-density voltage $j-V$ characteristics under simulated AM1.5G illumination (1000 W m^{-2}) of polymer/$PC_{70}BM$ solar cells is plotted in Figure 1a. We systematically observed that V_{oc} at 1 sun illumination results in higher values for cells processed with PCDTBT because of the more negative value of the HOMO respect to the vacuum level.[12a] In good accordance with recent works,[15] low bandgap character of DPP860 is observed in the absorption spectrum onset situated near 860 nm (see Figure 1b). This enlarged absorption produces a higher photocurrent as listed in Table 1.

To separate the influence of the charge carrier recombination process on the achievable V_{oc} from the aforementioned effect of the donor HOMO level position, we have performed a series of impedance measurements in polymer/$PC_{70}BM$ BHJ solar cells by varying the applied voltage at 1 sun irradiation intensity. The method to extract resistive (R_{rec} recombination resistance) and capacitive (C_μ chemical capacitance) parameters from impedance measurements was addressed in previous papers.[7a,16] We show in Figure 2 the variation of R_{rec} and C_μ as a function of the

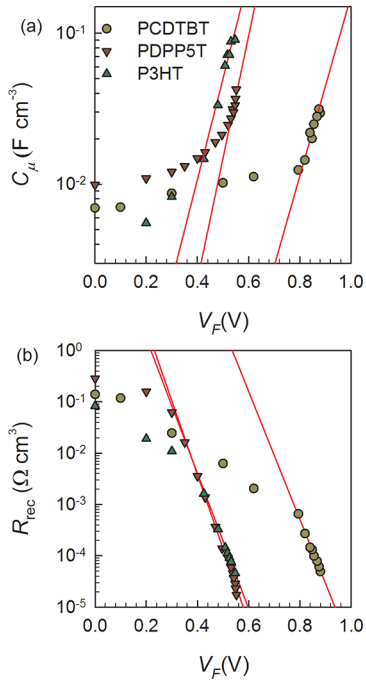

Figure 2. (a) Comparison of specific chemical capacitance−voltage response of polymer/$PC_{70}BM$-processed devices extracted from impedance analysis. Straight lines correspond to exponential fits as $C_\mu = C_0 \exp(\alpha q V_F/k_B T)$. (b) Specific recombination resistance R_{rec} as a function of the voltage. Straight lines correspond to exponential fits as $R_{rec} = R_0 \exp(-q\beta V_F/k_B T)$. In both plots the applied voltage V_{app} is assimilated to V_F.

voltage. At low voltages the measured capacitance responds to a dielectric mechanism. It is originated by the voltage-modulation of the depletion zone built up at the cathode contact, which collapses to the geometrical capacitance near zero voltage, as has been shown in our previous work.[16a] The analysis is particularly useful for solar cells in which there is no severe limitation to the charge transport.[14] By examining Figure 2, one can observe that for larger voltages the chemical capacitance exhibits the expected variation on voltage originated by the carrier occupation of electron density-of-states (DOS), $g(E)$ as $C_\mu = q^2 L g(V_F)$,[16a] L being the active layer thickness. It has been shown that in many cases electrons form a sort of minority carrier due to p-doping.[17] This makes the measured capacitance sensitive to the rise of the occupancy of electron states in the molecular acceptor. The occupancy of bandgap states is modulated by a parameter α, which accounts for the

dx.doi.org/10.1021/jp402751v | J. Phys. Chem. C 2013, 117, 8719−8726

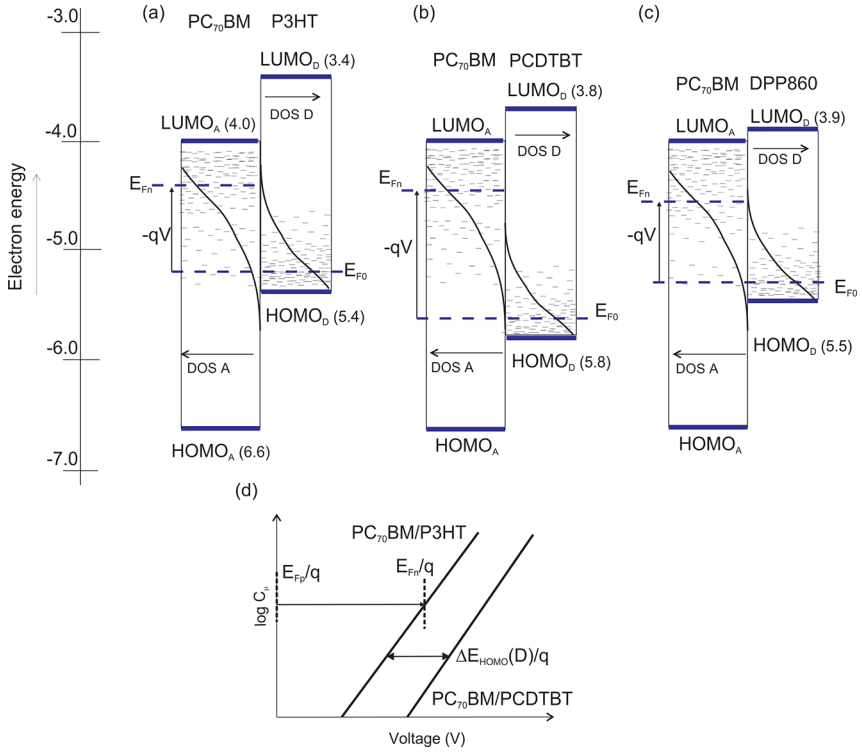

Figure 3. Energy diagram representing the polymer HOMO and fullerene LUMO manifolds (DOS) indicating the central value of the distribution. (a) P3HT HOMO level is estimated from CV analysis (Supporting Information). (b) PCDTBT and (c) DPP860 HOMO levels calculated from the shift of the capacitance−voltage plot. The procedure is illustrated in (d). Polymer LUMO levels are estimated from the tail of the absorption spectra in Figure 1b. The origin of the photovoltage is indicated.

characteristic energy of the DOS $\alpha=T/T_0$, being T_0 the characteristic temperature of the exponential distribution

$$g(E) = \frac{N_L}{k_B T_0} \exp[(E - E_{LUMO})/k_B T_0] \quad (2)$$

N_L stands for the total level density of the acceptor LUMO manifold. The equilibrium value of the carrier density is given by

$$n_0 = N_L \exp\left(\frac{E_{F0} - E_{LUMO}}{k_B T_0}\right) \quad (3)$$

which depends on the position of the equilibrium Fermi level E_{F0}. In zero-temperature approximation, the total electron carrier density is given by the integration of DOS up to the Fermi level

$$\begin{aligned} n &= \int_0^{E_{Fn}} g(E)\mathrm{d}E \\ &= N_L \exp\left(\frac{E_{Fn} - E_{LUMO}}{k_B T_0}\right) \\ &= n_0 \exp\left(\frac{E_{Fn} - E_{F0}}{k_B T_0}\right) \end{aligned} \quad (4)$$

It is observed in Figure 2a that C_μ exhibits an exponential dependence at high voltages, that is, $C_\mu = C_0 \exp(\alpha q V_F/k_B T)$, with $\alpha \approx 0.3$–0.4 (see Table 1). C_μ extracted from the impedance analysis is then a replica of the bandgap electronic state distribution as the occupation progresses following the Fermi level displacement.[17a]

It is also useful to introduce the carrier density in a transport level at the energy E_c

$$n_c = n_c^0 \exp\left(\frac{E_{Fn} - E_{F0}}{k_B T}\right) \quad (5)$$

Equation 5 is most useful in the case of a multiple trapping mechanism in which a sharp distinction can be made between free and trapped electrons. The special feature of the carriers at the transport level is that charge density relates simply to the voltage V_F as

$$n_c = n_c^0 \exp\left(\frac{qV_F}{k_B T}\right) \quad (6)$$

This last equation assumes that the majority carrier concentration is not significantly modified so that $E_{Fp} \approx E_{F0}$. Because actual measurements are often performed as a function of voltage, the free carrier density is a useful index of the voltage V_F, in order to formulate a recombination model. In general, the experimental relevance of a free carrier density must be proved by transport measurements, and one relies on the total carrier density introduced in eq 4. For the case of an exponential distribution of traps, one can convert from free to total carrier density by the expression

$$\frac{n}{n_0} = \left(\frac{n_c}{n_c^0}\right)^\alpha \quad (7)$$

By combining eqs 6 and 7, the total carrier density reproduces the slope of the experimental exponential behavior found in the capacitance as $n = n_0 \exp(\alpha q V_F/k_B T)$ in accordance with eq 4. The DOS occupancy (identified from

dx.doi.org/10.1021/jp402751v | J. Phys. Chem. C 2013, 117, 8719−8726

the exponential rise in the chemical capacitance) is shifted in energy depending on the polymer HOMO position with respect to the acceptor LUMO level. In the devices studied here, the same acceptor fullerene is used so that it is reasonable to relate the voltage shift in the capacitance plot of Figure 2a principally to the polymer HOMO level offset. To take P3HT HOMO as a reference CV analysis has been performed giving a value ∼−5.4 eV (see Supporting Information) within the range found in previous works.[18] We adopt the criterion of extracting the HOMO level from the maximum of the oxidation peak (DOS center). This criterion situates the oxidation peak onset on the tail of the DOS (∼−5.2 eV) and, consequently, within the effective bandgap energies. The energy disorder broadens the HOMO manifold being the DOS center a measurement of the HOMO level mean. This is illustrated in Figure 3.

The voltage shift in Figure 2a is then interpreted in terms of the polymer HOMO offset, as drawn in Figure 3d. By taking this voltage shift and the HOMO reference value for P3HT a value of −5.5 eV for DPP860 HOMO can be calculated, and lower position is derived for PCDTBT HOMO (−5.8 eV).[12a] As explained previously, these values indicate the DOS center rather than the onset of state occupancy. From the absorption spectra in Figure 1b, the energy diagram in Figure 3 is derived. We remark here that the capacitive method reported allows establishing the polymer HOMO position in complete cells when a reference is known and measured using alternative techniques.

Resistive Response and Recombination Kinetics. The differential resistance R_{rec} extracted from impedance conveys information about the recombination flux. Recombination of excess carriers is phenomenologically modeled as

$$j_{rec} = j_0\left[\left(\frac{n_c}{n_c^0}\right)^{\beta} - 1\right] = j_0\left[\exp\left(\beta\frac{qV_F}{k_BT}\right) - 1\right] \quad (8)$$

The expression in eq 8 for the recombination current is usually labeled as the β-recombination model that includes the parameter β accounting for the deviation from the ideal diode equation (inverse of the diode ideality factor), being j_0 the dark, saturation recombination current.[19] Recombination resistance is defined from the recombination current derivative[7a]

$$R_{rec} = L\left(\frac{dj_{rec}}{dV_F}\right)^{-1} \quad (9)$$

By examining Figure 2b, one can infer that the recombination resistance corresponds to an approximate exponential behavior $R_{rec} = R_0 \exp(-\beta q V_F/k_BT)$, as expected from the eq 8 derivative in the case of high injection. A straightforward estimation of the β-parameter is obtained that results in $\beta \approx 0.7-0.8$ (see Table 1). At lower voltages R_{rec} tends to saturate presumably because the differential resistance measured is not only determined by the recombination flux but also by a shunt resistance caused by additional parallel leakage currents.

Equation 8 can be alternatively written in terms of a power-law dependence of the total carrier density as

$$j_{rec} = qLB[n^{\gamma} - {n_0}^{\gamma}] \quad (10)$$

where B represents a recombination coefficient that establishes the time scale for recombination kinetics.

The excess electron n density appears in addition to background equilibrium electron density n_0. In the dark, the equilibrium densities produce the saturation recombination current that compensates the thermal generation,

$$j_0 = qLB{n_0}^{\gamma} \quad (11)$$

However, actual measurement of the reverse current in the dark may not provide j_0 due to leakage currents. From eq 7 we obviously have the relationship $\gamma = \beta/\alpha$.

By looking at α and β values extracted from experiments (Table 1), it is observed that $\beta \approx 2\alpha$ is satisfied within the experimental error. The γ exponent results then in values approximately around 2. In the case of DPP860, a slightly lower exponent is found, $\gamma = 1.77$. This experimental fact lets us write eq 8 as $j_{rec} \propto n^{\gamma}$, with $\gamma \approx 2$, signaling an approximate bimolecular-like behavior for the recombination process in good accordance with the electroneutrality condition $n = p$. It has been identified in some studies based on impedance spectroscopy that $\gamma \approx 2$,[7a,20] while transient analyses usually give $\gamma \geq 2$.[2,21]

From eqs 8 and 9 we derived that the recombination current can be written in terms of the recombination resistance as $j_{rec} = k_BT/\beta q R_{rec}$,[14] that allows for a straightforward calculation of the recombination coefficient B based on differential resistive and capacitive parameters extracted from impedance spectroscopy. By combining eqs 8 and 4 in the case of high injection, one arrives at

$$B = \frac{k_BT}{q^2Ln^2\beta R_{rec}} \quad (12)$$

The derivation of eq 12 assumes a rather constant value for the recombination coefficient, nearly independent of energetics of the states taking part on the recombination event. Results of applying eq 12 are shown in Figure 4. It is observed that for V_F > 0.4 V the recombination coefficient for each blend does exhibit an almost constant behavior always within the range of $B \approx 10^{-12}-10^{-11}$ cm^3 s^{-1}. In the case of P3HT/PC$_{70}$BM devices, a lower coefficient $B = 2 \times 10^{-12}$ cm^3 s^{-1} is encountered in comparison with PCDTBT/PC$_{70}$BM ($B = 2 \times 10^{-11}$ cm^3 s^{-1}), and DPP860/PC$_{70}$BM ($B \approx 6 \times 10^{-11}$ cm^3 s^{-1}) solar cells. For lower voltages, B departs from the approximate constant value because both R_{rec} and C_μ largely deviate from the exponential behavior. It is worth noting that recombination coefficient values found for P3HT and PCDTBT are in good agreement with recent results obtained using alternative techniques.[22] In addition, results in Figure 4

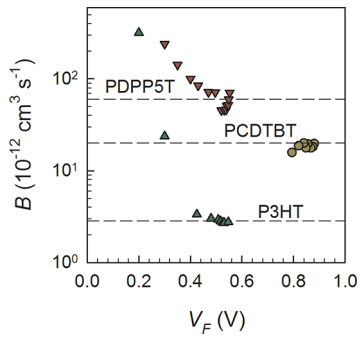

Figure 4. Recombination coefficient B calculated by means of eq 12 using the parameters extracted from the impedance analysis. Horizontal dashed lines mark average values of data points following the exponential behavior in Figure 2.

dx.doi.org/10.1021/jp402751v | J. Phys. Chem. C 2013, 117, 8719−8726

Table 2. Recombination Coefficient B Extracted from Impedance Analysis[a]

	B (cm^3 s^{-1})	j_0 (A cm^{-2})	j_{0k} (A cm^{-2})	N_{00} (cm^{-3})	V_{if} (meV)	ΔV_{oc}^{kin} (mV)	V_{oc}' (mV)
P3HT	2×10^{-12}	4.7×10^{-10}	1.7×10^{4}	7.8×10^{19}	0.09		
PCDTBT	2×10^{-11}	7.8×10^{-14}	3.9×10^{4}	3.5×10^{19}	0.19	85	875
DPP860	$\sim 6 \times 10^{-11}$	1.5×10^{-10}	2.7×10^{6}	1.7×10^{20}	0.70	110	550

[a]Saturation current, j_0, and exponential prefactor, j_{0k} in eq 13. Total level density N_{00}, calculated from eq 14, and resulting electronic coupling V_{if}. ΔV_{oc}^{kin} corresponding to the kinetic term in eq 20b. V_{oc}' calculated with eq 20, taking V_{oc} of P3HT-based cells as reference.

point to the fact that the energy location of recombining carriers within the DOS has a minor influence on the recombination coefficient value.

Connection to Molecular Charge Transfer Parameters. A key parameter to understand the kinetics of charge carrier recombination in solar cells is the saturation current j_0 in eq 8.[10b,23] It is known that j_0 establishes the time scale of recombination through the combined effect of the charge transfer energetics and kinetics. As suggested for inorganic semiconductors,[23a] one can propose a separation of the form

$$j_0 = j_{0k} \exp\left(-\frac{\beta E_g}{k_B T}\right) \tag{13}$$

An expression that explicitly separates kinetic terms represented by the prefactor j_{0k} from energetic contributions stated through bandgap energy E_g. In inorganic materials, E_g is a single function of the semiconductor. However, in organic blends the effective gap $E_g = E_{LUMO}(A) - E_{HOMO}(D)$ is a function of the relative energetics of the blend components. Therefore, assessing the influence of energetics on j_0 is a matter that requires careful investigation. In accordance to the capacitance dependence on voltage, we propose a background equilibrium carrier density as $N_0 = N_{00} \exp(-\alpha E_g/k_B T)$, being N_{00} a parameterer accounting for the total level density. It is worth noting that the last expression is consistent with eq 13 and the form adopted by j_0 previously introduced in eq 11. Such identification readily allows connecting j_{0k} and B as

$$j_{0k} = qLBN_{00}^{\gamma} \tag{14}$$

Our approach permits evaluating j_{0k} directly from the impedance analysis rather than from the $j-V$ characteristic usually masked by leakage currents at low bias voltages. Equation 13 and fittings of the recombination resistance in Figure 2b provide the value for j_0 (see Table 2). Blends with larger effective gap yields lower j_0 values, as expected. It is feasible to determine j_{0k} taking into account the effective gap, as derived from the capacitance voltage shift. It is observed in Table 2 that j_{0k} qualitatively follows the trend exhibited by B, confirming the higher recombining character of DPP860-based cells. A consistency proof relies upon evaluating N_{00} taking into account the relationship in eq 14. By examining Table 2, one can observe that N_{00} encountered is within the range of $10^{19}-10^{20}$ cm^{-3}, in good agreement with the total density of active molecules in the active layer.

These findings are a strong indication that the recombination kinetics does not depend on the absolute energetics of the donor HOMO levels. Indeed, deeper HOMO positions, as is the case of PCDTBT (−5.8 eV), result in recombination coefficients in between those observed for much lower ionization energy polymers as P3HT (−5.4 eV) and DPP860 (−5.5 eV). Some approaches, connected to the original Langevin theory on the recombination in single phases, related recombination coefficient B_L directly to the carrier mobility μ exhibited by electrons and holes as $B_L = q\mu/\varepsilon$.[9b] This gives a volumetric recombination flux as $U_L = B_L np$. Understanding the reported recombination coefficient values in Figure 4 in terms of transport features, as derived from Langevin-like recombination approaches is difficult. Similar electron mobilities are expected because of the use of the same fullerene, and it is not evident how DPP380 exhibits more than 1 order of magnitude greater hole mobility than P3HT to explain faster recombination.

An alternative view regards the charge transfer event itself as the limiting rate factor of the recombination mechanism. It is then the specific molecular environment at donor−acceptor interfaces that sates the time scale for recombination. In a previous work[20] we have reported on the small dependence of the recombination kinetics on the fullerene electron affinity and voltage. It was concluded within the framework of the Marcus theory that the reorganization energy, λ, rather than the polymer HOMO/fullerene LUMO energy offset or the DOS occupancy level, takes control over the charge transfer event. The charge transfer rate k_0 in the semiclassical Marcus expression is written as

$$k_0 = \frac{2\pi}{\hbar} |V_{if}|^2 \sqrt{\frac{1}{4\pi\lambda k_B T}} \exp\left(-\frac{(\Delta G_0 + \lambda)^2}{4\lambda k_B T}\right) \tag{15}$$

where ΔG_0 is the variation of the Gibbs free energy during the reaction and V_{if} corresponds to the electronic coupling matrix element (charge transfer integral) between initial and final states. We identify here ΔG_0 with the acceptor and donor energy level offset, $\Delta G_0 \sim E_n - E_p$.

In the experiments presented here, large variations in B (or equivalently j_{0k}) are observed among polymers, without any correlation with the polymer ionization energy. Recalling again the Marcus approach in eq 15, one can infer that, to slow down the recombination kinetics, small values of V_{if} and large λ are necessary. We note from Figure 4 that the recombination kinetics results slightly dependent on the voltage for a given polymer/fullerene combination. This behavior is in good agreement with a large value for $\lambda \approx 0.7$ eV, as stated in recent works.[20] This last observation would imply that the observed variation in B might be connected to changes in V_{if}, a parameter that mainly reflects the environment in which fullerene/polymer interfaces are located. It is known that it highly depends on both relative molecular orientations and intermolecular distances.[11a] By comparing eq 14 and eq 15, one can readily arrive at $k_0 = BN_{00}$ because $\gamma = 2$ as noted previously. This last identification allows us to calculate V_{if}, assuming that the charge transfer event occurs closely to the maximum rate, in accordance with a large reorganization energy. Under this assumption, the exponential term in eq 15 is close to 1, and it can be obtained that $|V_{if}|^2 = Bn_{00}\hbar(4\pi\lambda k_B T/2\pi)$. The calculated electronic coupling matrix V_{if} values are listed in Table 2. One can observe that when very low, <1 meV, values are found, it signals the high inhibiting character of the

dx.doi.org/10.1021/jp402751v | J. Phys. Chem. C 2013, 117, 8719−8726

recombination charge transfer between reduced fullerene molecules and oxidized polymer units.[24] Nevertheless, the relatively more recombining blend containing DPP860 exhibits larger V_{if} value in comparison with the other combinations studied.

Determination of Energy Losses. The previous analysis based on impedance measurements allows for an estimation of the actual donor HOMO level considering the P3HT HOMO as a well-established reference. Taking into account the recombination current in eq 8, a useful representation of the $j-V$ characteristics results by including the photocurrent term j_{ph},

$$j = j_0\left[\exp\left(\beta\frac{qV_F}{k_BT}\right) - 1\right] - j_{ph} \tag{16}$$

At V_{oc}, the saturation current is largely exceeded by the recombination term in eq 8, and assuming a voltage-independent photocurrent $j_{ph} = j_{sc}$, one readily arrives at

$$V_{oc} = \frac{k_BT}{q\beta}\ln\left(\frac{j_{sc}}{j_0}\right) \tag{17}$$

Equation 17 entails that variations in V_{oc} are linked with two different contributions. Higher photocurrent increases V_{oc} because photogenerated carrier density attains larger values. On the contrary, lower dark current j_0 reduces the recombination flux also allowing for an increment in the photogenerated carriers. This is because solar cells function under the principle of the kinetic balance between light-induced carrier generation and recombination. The detrimental effect of increased recombination on V_{oc} can be easily quantified. We notice that the term related to differences in short-circuit current as $k_BT/q\beta\ \ln(j_{SC}'/j_{SC})$ only amounts about 15 meV when DPP860- and P3HT-based cells are compared so that it can be omitted in the following calculations. From eq 17 it is derived that

$$\Delta V_{oc} = \frac{k_BT}{q\beta}\ln\left(\frac{j'_0}{j_0}\right) \tag{18}$$

In eq 18, ΔV_{oc} stands for the V_{oc} enhancement (for the less recombining cell) owed to the reduction in dark current recombination j_0 with respect to the value exhibited by the more recombining cell j'_0. Hence, using eq 11 one can separate two contributions in eq 17 as

$$\Delta V_{oc} = \frac{k_BT}{q\beta}\left[\ln\left(\frac{B'}{B}\right) + \ln\left(\frac{n'_0{}^{\gamma}}{n_0{}^{\gamma}}\right)\right] \tag{19}$$

The first summand $k_BT/q\beta\ln(B'/B)$ is easily interpreted as a V_{oc} loss owed exclusively to the difference in the recombination kinetics. The second summand $k_BT/q\beta\ \ln(n_0'^{\gamma}/n_0^{\gamma})$, which derives from a ratio between equilibrium carrier densities, can be expressed in terms of the effective bandgap. This term represents the essential influence of the energetics on the recombination kinetics. As stated in eq 2, the equilibrium carrier density n_0, which determines the saturation current j_0, scales with the equilibrium Fermi level E_{F0}. Recalling eq 2 and taking into account that the energy shift in E_{F0} is caused by the polymer HOMO level offset a separation of kinetics and energetics terms in eq 19 is derived

$$\Delta V_{oc} = \Delta V_{oc}^{kin} + \Delta V_{oc}^{ener} \tag{20a}$$

where

$$\Delta V_{oc}^{kin} = \frac{k_BT}{q\beta}\ln\left(\frac{B'}{B}\right) \tag{20b}$$

$$\Delta V_{oc}^{ener} = \frac{E_{HOMO}(D) - E'_{HOMO}(D)}{q} \tag{20c}$$

Equation 20a explicitly states that V_{oc} variations among solar cells comprising different active materials can be simply split into two separated contributions: one related to differences in recombination kinetic time scale, the other exclusively linked with energy HOMO offset of the donors, as far as N_{00} exhibits similar values between the compared cells. The case of comparing acceptors with different LUMO level has been recently treated.[20] If only the recombination kinetics term of eq 20b is considered one can arrive at quantifying a significant loss in open-circuit voltage of about 100 meV (Table 2) exclusively produced by the increment in the recombination kinetics exhibited by PCDTBT- and DPP860-based solar cells in comparison to that occurring for less recombining P3HT-based devices. Such a shift in V_{oc} caused by recombination losses entails power conversion efficiency reduction approximately equal to 20% in the case of DPP860 used as donor polymer. Moreover, the application of eq 20 allows us to determine $V'_{oc} = V_{oc} - \Delta V_{oc}$, taking the values exhibited by P3HT-based cell as reference. Estimation of V_{oc} lies within the experimental error as observed in comparing Table 1 and Table 2.

4. CONCLUSION

We have demonstrated how electronic coupling at polymer/fullerene interfaces can have a determining influence on the kinetics of charge carrier recombination in a variety of bulk-heterojunction solar cells containing polymers of different ionization energy and absorption properties. Although transport properties have been regarded to govern carrier recombination by establishing the rate limiting mechanism, our findings situate the focus on the inner interfacial properties of the photovoltaic blends. Rather there exists a correlation between the loss in open-circuit voltage and the molecular electronic coupling of the donor/acceptor system. As derived from the Marcus approach for charge transfer, recombination in an efficient solar cell needs for reduced electronic coupling and large reorganization energy between initial and final states. Our analysis corroborates such requirements ($V_{if} < 1$ meV and $\lambda \approx 0.7$ eV) being differences in recombination coefficient connected to variations in the electronic coupling among blends. We note that a detailed knowledge about both relative molecular orientations and intermolecular distances at polymer/fullerene interfaces could be used as a fruitful guide for improvement of organic solar cell performance.

■ ASSOCIATED CONTENT

Supporting Information

CV analysis for the determination of the energy reference of P3HT HOMO level. This material is available free of charge via the Internet at http://pubs.acs.org.

■ AUTHOR INFORMATION

Corresponding Author

*E-mail: garciag@fca.uji.es.

Notes

The authors declare no competing financial interest.

■ ACKNOWLEDGMENTS

This work was partially supported by FP7 European Collaborative Project SUNFLOWER (FP7-ICT-2011-7, Contract No. 287594), Ministerio de Educacion y Ciencia (Spain), under Project HOPE CSD2007-00007 (Consolider-Ingenio 2010), and Generalitat Valenciana (Prometeo/2009/058 and ISIC/2012/008 Institute of Nanotechnologies for Clean Energies).

■ REFERENCES

(1) Green, M. A.; Emery, K.; Hishikawa, Y.; Warta, W.; Dunlop, E. D. *Prog. Photovoltaics: Res. Appl.* **2012**, *20*, 12−20.
(2) Maurano, A.; Hamilton, R.; Shuttle, C. G.; Ballantyne, A. M.; Nelson, J.; O'Regan, B.; Zhang, W.; McCulloch, I.; Azimi, H.; Morana, M.; Brabec, C. J.; Durrant, J. R. *Adv. Mater.* **2010**, *22*, 4987−4992.
(3) Garcia-Belmonte, G.; Bisquert, J. *Appl. Phys. Lett.* **2010**, *96*, 113301.
(4) Kaake, L. G.; Barbara, P. F.; Zhu, X.-Y. *J. Phys. Chem. Lett.* **2010**, *1*, 628−635.
(5) Jamieson, F. C.; Domingo, E. B.; McCarthy-Ward, T.; Heeney, M.; Stingelin, N.; Durrant, J. R. *Chem. Sci.* **2012**, *3*, 485−492.
(6) (a) Wienk, M. M.; Turbiez, M.; Gilot, J.; Janssen, R. A. J. *Adv. Mater.* **2008**, *20*, 2556−2560. (b) Boix, P. P.; Wienk, M. M.; Janssen, R. A. J.; Garcia-Belmonte, G. *J. Phys. Chem. C* **2011**, *115*, 15075−15080.
(7) (a) Garcia-Belmonte, G.; Boix, P. P.; Bisquert, J.; Sessolo, M.; Bolink, H. J. *Sol. Energy Mater. Sol. Cells* **2010**, *94*, 366−375. (b) Credgington, D.; Durrant, J. R. *J. Phys. Chem. Lett.* **2012**, *3*, 1465−1478.
(8) Kuik, M.; Koster, L. J. A.; G. A. H. Wetzelaer, G. A. H.; Blom, P. W. M. *Phys. Rev. Lett.* **2011**, *107*, 256805.
(9) (a) Koster, L. J. A.; Mihailetchi, V. D.; Blom, P. W. M. *Appl. Phys. Lett.* **2006**, *88*, 052104. (b) Deibel, C.; Wagenpfahl, A.; Dyakonov, V. *Phys. Rev. B* **2009**, *80*, 075203.
(10) (a) Schlenker, C. W.; Thompson, M. E. *Chem. Commun.* **2010**, *47*, 3702−3716. (b) Yamamoto, S.; Orimo, A.; Ohkita, H.; Benten, H.; Ito, S. *Adv. Energy Mater.* **2012**, *2*, 229−237.
(11) (a) Yi, Y.; Coropceanu, V.; Bredas, J.-L. *J. Am. Chem. Soc.* **2009**, *131*, 15777−15783. (b) Ko, S.; Hoke, E. T.; Pandey, L.; Hong, S.; Mondal, R.; Risko, C.; Yi, Y.; Noriega, R.; McGehee, M. D.; Brédas, J.-L.; Salleo, A.; Bao, Z. *J. Am. Chem. Soc.* **2012**, *134*, 5222−5232.
(12) (a) Blouin, N.; Michaud, A.; Leclerc, M. *Adv. Mater.* **2007**, *19*, 2295−2300. (b) Park, S. H.; Roy, A.; Beaupré, S.; Cho, S.; Coates, N.; Moon, J. S.; Moses, D.; Leclerc, M.; Lee, K.; Heeger, A. J. *Nat. Photonics* **2009**, *3*, 297−302. (c) Alem, S.; Chu, T.-Y.; Tse, S. C.; Wakima, S.; Lu, J.; Movileanu, R.; Tao, Y.; Bélanger, F.; Désilets, D.; Beaupré, S.; Leclerc, M.; Rodman, S.; Waller, D.; Gaudiana, R. *Org. Electron.* **2011**, *12*, 1788−1793.
(13) Gevaerts, V. S.; Furlan, A.; Wienk, M. M.; Turbiez, M.; Janssen, R. A. J. *Adv. Mater.* **2012**, *24*, 2130−2134.
(14) Boix, P. P.; Guerrero, A.; Marchesi, L. F.; Garcia-Belmonte, G.; Bisquert, J. *Adv. Energy Mater.* **2011**, *1*, 1073−1078.
(15) Wienk, M. M.; Turbiez, M.; Gilot, J.; Janssen, R. A. J. *Adv. Mater.* **2008**, *20*, 2556−2560.
(16) (a) Fabregat-Santiago, F.; Garcia-Belmonte, G.; Mora-Seró, I.; Bisquert, J. *Phys. Chem. Chem. Phys.* **2011**, *13*, 9083−9118. (b) Garcia-Belmonte, G.; Guerrero, A.; Bisquert, J. *J. Phys. Chem. Lett.* **2013**, *4*, 877−886.
(17) (a) Bisquert, J.; Garcia-Belmonte, G. *J. Phys. Chem. Lett.* **2011**, *2*, 1950−1964. (b) Li, J. V.; Nardes, A. M.; Liang, Z.; Shaheen, S. E.; Gregg, B. A.; Levi, D. H. *Org. Electron.* **2011**, *12*, 1879−1885.
(18) (a) Hou, J.; Chen, T. L.; Zhang, S.; Huo, L.; Sista, S.; Yang, Y. *Macromolecules* **2009**, *42*, 9217−9219. (b) Gong, X.; Tong, M.; Brunetti, F. G.; Seo, J.; Sun, Y.; Moses, D.; Wudl, D.; Heeger, A. J. *Adv. Mater.* **2011**, *23*, 2272−2277. (c) Greaney, M. J.; Das, S.; Webber, D. H.; Bradforth, S. E.; Brutchey, R. L. *ACS Nano* **2012**, *6*, 4222−4230.
(19) Bisquert, J.; Mora-Seró, I. *J. Phys. Chem. Lett.* **2010**, *1*, 450−456.
(20) Guerrero, A.; Marchesi, L. F.; Boix, P. P.; Bisquert, J.; Garcia-Belmonte, G. *J. Phys. Chem. Lett.* **2012**, *3*, 1386−1392.
(21) Shuttle, C. G.; O'Regan, B.; Ballantyne, A. M.; Nelson, J.; Bradley, D. D. C.; de Mello, J.; Durrant, J. R. *Appl. Phys. Lett.* **2008**, *92*, 093311.
(22) (a) Etzold, F.; Howard, I. A.; Mauer, R.; Meister, M.; Kim, T.-D.; Lee, K.-S.; Baek, N. S.; Laquai, F. *J. Am. Chem. Soc.* **2011**, *133*, 9469−9479. (b) Clarke, T. M.; Peet, J.; Nattestad, A.; Drolet, N.; Dennler, G.; Lungenschmied, C.; Leclerc, M.; Mozer, A. J. *Org. Electron.* **2012**, *13*, 2639−2646.
(23) (a) Sze, S. M. *Physics of Semiconductor Devices*, 2nd ed.; John Wiley & Sons: New York, 1981; (b) Enwin, P.; Thompson, M. E. *Appl. Phys. Lett.* **2011**, *98*, 223305.
(24) Yi, Y.; Coropceanu, V.; Bredas, J.-L. *J. Mater. Chem.* **2011**, *21*, 1479−1486.